THE JOURNAL OF PHYSICAL CHEMISTRY C

Article

Cite This: J. Phys. Chem. C 2018, 122, 22424−22434

pubs.acs.org/JPCC

Reversible Olefin Addition to Extended Lattices of a Nickel−Selenium Framework

Dušan N. Sredojević,*[,†,‡] Salvador Moncho,[†] Rajesh Kumar Raju,[†] Milivoj R. Belić,[†] and Edward N. Brothers*[,†]

[†]Science Program, Texas A&M University at Qatar, Texas A&M Engineering Building, Education City, 23874 Doha, Qatar

[‡]Institute of Nuclear Sciences, Vinča, University of Belgrade, P.O. Box 522, 11001 Belgrade, Serbia

Supporting Information

ABSTRACT: We performed density functional theory computations to study the structural and electronic properties as the basis of ethylene addition activity for $[Ni(XC)_4]_n$ (X = Se, S)-extended lattices. We demonstrated that the mechanism of ethylene cycloaddition to a periodic $[Ni(SeC)_4]_n$ two-dimensional (2D) network is analogous to that previously described for $[Ni(SC)_4]_n$ 2D sheets and similar to the metal bis(dithiolene) molecular complexes $[M(S_2C_2R_2)_2]$ (M = Ni, Pd, Pt, Co, Cu). These nanosheet materials avoid decomposition upon olefin addition, which is one of the main limitations of the molecular metal bis(dithiolene) complexes, as we find the decomposition processes to be thermodynamically unfavorable. Our calculations also suggest that the preferred conformation of the $[Ni(SeC)_4]_n$ bilayer lattice is parallel displaced, with the Se atoms positioned above the Ni atoms, which is different from the eclipsed conformation found for $[Ni(SC)_4]_n$. We also managed to optimize an adduct of $[Ni(SC)_4]_n$ in the bilayer form, which exceed the ethylene coverage of molecular complexes. We calculate that the preferred three-dimensional geometry of the stacked sheets is eclipsed because of strong van der Waals interactions. Such an arrangement of the sheets indicates that these materials should be highly porous, pointing to the high capacity for olefin bindings. Indeed, a few moderately stable ethylene adducts have been located. Owing to their unique structures and chemical reactivity, these newly predicted materials can be potentially developed as electrocatalysts for olefin purification.

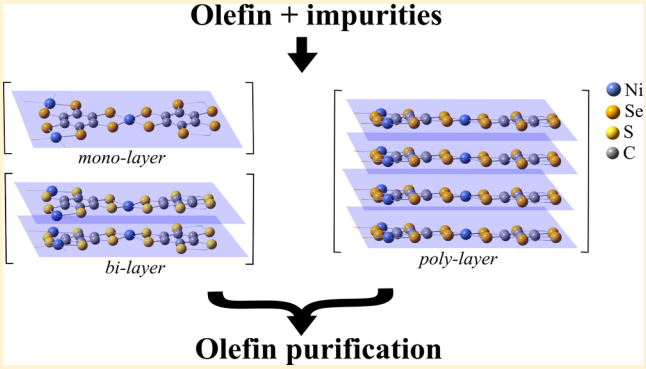

INTRODUCTION

Pure olefins represent some of the most important precursors in the chemical industry, as they are broadly used in the production of various chemicals such as alcohols, ethers, esters, acids, and different polymers.[1,2] Because they appear as a mixture with other organic components in the petrochemical feedstock, especially with paraffins and sulfide contaminants, the separation and purification of olefins represent pivotal engineering steps in their preparation. The current approach for olefin separation relies on cryogenic distillation, which makes the overall process of olefin production quite expensive.[3] Thus, there is a need to develop alternative/cheaper methods. Some studies have suggested the application of transition metals; however, Cu(I) and Ag(I) as olefin carriers through reversible bindings have found their practical use limited because of the deactivation caused by common impurities (H_2O, H_2S, CO, acetylene, etc.).[4,5]

A more promising method was proposed by Wang and Stiefel, who utilized an electrochemical system based on the nickel bis(dithiolene) complexes ($Ni(S_2C_2R_2)$).[6] The advantage of these complexes, compared to those previously reported, is in their inactivity to molecules recognized as common impurities, which makes them highly selective for olefin binding. A procedure has been developed that reversibly binds olefins to nickel dithiolenes under controlled conditions; the release of olefins is controlled via electrochemical reduction. Crystallographic characterization revealed that the products of olefin addition to nickel bis(dithiolene) complexes contain two $S_{ligand}-C_{olefin}$ bonds.[6−10] Therefore, these reactions can be viewed as a nucleophilic cycloaddition of C═C bond to the bis(dithiolene) complexes.

Our aim here is to predict the structure of an advanced heterogeneous bis(dithiolene)-like catalyst that could be used for olefin purification, based on the strategy proposed by Wang and Stiefel, but with improved characteristics. Many attempts have been made in order to theoretically anticipate the structure of metal dithiolenes or analogues, with potential applications in homogeneous catalysis, based on the previously described mechanisms of olefin addition.[11−19] However, these homogeneous catalysts would often entail different practical

Received: June 14, 2018
Revised: September 12, 2018
Published: September 13, 2018

DOI: 10.1021/acs.jpcc.8b05707
J. Phys. Chem. C 2018, 122, 22424−22434

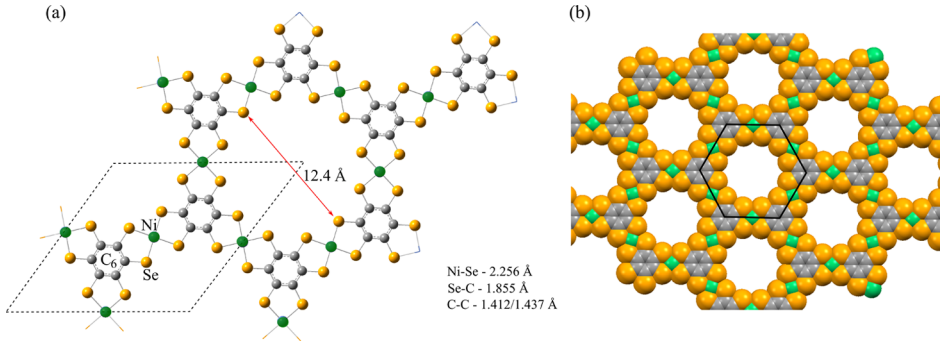

Figure 1. (a) Optimized structure of the $[Ni(SeC)_4]_n$ 2D sheet calculated at the HSE06/DZ level of theory. The unit cell is delimited by the dashed rhombus, whereas the red double arrow gives the large pore size. (b) Space-fill representation of 2D hexagons is drawn using Mercury.[41] Ni, Se, and C atoms are presented as green, orange-brown, and gray spheres, respectively.

limitations, such as the tendency to decompose in the reaction with olefins, show low olefin-to-metal complex binding ratio (1:1), as well as practical complexity of the separation procedure. To avoid such practical disadvantages of metal dithiolenes as potential homogeneous catalysts, we turn our attention toward investigating analogous heterogeneous catalysts.[20] In particular, we turn to materials inspired by the work of Kambe and co-workers, who have recently synthesized a two-dimensional (2D) material which contains NiS_4 motifs networked with the C_6 aromatic units.[21] This planar nanosheet material exhibits an extended π-conjugation over the Ni bis(dithiolene)/benzene units within the framework of a hexagonally ordered structure. Considering that similar 2D materials (atomically thin), such as graphene,[22−24] hexagonal BN sheets,[25−28] and analogues, have recently made significant inroads into various nanotechnologies, it is reasonable to expect that nickel dithiolene based nanosheet materials will also capture much attention soon, owing to their unique electronic and mechanical properties that have been thus far uncovered.[29]

From our perspective, the most intriguing feature of this material is its potential reactivity with olefins that was predicted in a study based on the density functional theory (DFT).[30] In our previous work, we studied the possible reaction pathways, using an appropriate hybrid functional applicable to periodic system (HSE06) for that purpose, knowing that the pure density functional overstabilizes the reaction barriers.[31] A new low-laying energy pathway for the olefin addition onto this material was discovered. We also examined some additional binding motifs from the molecular system point of view (such as ethylene binding to nickel and coordinated sulfur), as well as new motifs that are only possible in 2D arrangements (such as ethylene binding to two sulfur atoms of adjacent chelate rings of the same C_6 unit). This was the crucial point that revealed the potential efficiency of this material as a catalyst for olefin purification.[31]

In the present study, we use the same density functional (HSE06) in order to investigate the potential reactivity of an analogous $[Ni(SeC)_4]_n$ material toward the olefins and to compare it with the previously calculated energy profiles for the dithiolene-based π-conjugated nanosheet. We find that molecular nickel bis(diselenolene) is a promising alternative to the parent sulfur complex because of its very low barriers and stability versus the decomposition.

Inspired by a recent study, which revealed that the π-conjugated 2D $[Ni(SC)_4]_n$ material may exist in the form of bilayers rather than in the single-layer form,[32] we extended our investigation to include the bilayer and polylayer [three-dimensional (3D)] sulfur and selenium-based structures and examine their capability for ethylene binding. Furthermore, because of the well-known tendency of nickel bis(dithiolene) complexes to decompose in the reaction with olefins,[10] we have also theoretically studied the persistence of these materials against decomposition upon ethylene addition. This was done based on the model systems that are capable of reproducing multiple intraligand ethylene additions, by calculating the appropriate heights of the barriers, and comparing them to the proposed decomposition scheme for the molecular system.

COMPUTATIONAL DETAILS

We performed all calculations using the Gaussian 09 suite of programs.[33] All DFT calculations were done by employing the screened hybrid functional HSE06.[34−36] This functional has been chosen mostly because it uses an exact short-range exchange, avoiding any numerical issues that appear in the periodic boundary calculations (PBC) with the functional that includes a long-range exact exchange. In addition, this functional is advantageous over the pure functional, such as Perdew−Burke−Ernzerhof,[37] because it predicts the heights of the reaction barriers more accurately. All calculations were performed as closed shell, which considers nickel atoms in their singlet spin states. We have also performed the series of single-point calculations, so as to determine the preferred arrangement of hypothetical polylayered (3D) structures. For this purpose, we compared the HSE06-based results with those obtained by the pure Truhlar's functional (M06-L).[38] All calculations have been done by utilizing the def2-SVP basis set (hereafter called DZ),[39] which was previously confirmed to provide the results close to the ones obtained with a larger basis set def2-TZVPP (within 1 kcal/mol).[31] Numerical vibrational frequencies were calculated in order to confirm the nature of the intermediates or adducts (no imaginary frequency) and the transition states (only one imaginary frequency). The PBC calculations used 20 k points for both mono- and bilayered $[Ni(SC)_4]_n$/$[Ni(SeC)_4]_n$ structures, with unit cells that include three nickel atoms, whereas 116 k points were used for polylayered (3D) structures of the same unit cells.[40]

RESULTS AND DISCUSSION

We begin our study with the examination of the geometrical and electronic properties of the 2D nickel bis(diselenolene)-

DOI: 10.1021/acs.jpcc.8b05707
J. Phys. Chem. C 2018, 122, 22424−22434

based lattice. The optimization of such a structure yields a porous cross-linked planar $Ni(SeC)_4$ network, with the Ni−Se covalent bonds defining the square-planar coordination of the nickel center (Figure 1). This structure can be viewed as 2D fused hexagons, with $NiSe_4$ centers as the sides and C_6 rings as the vertices. The optimized lattice parameter of the unit cell (dashed lines in Figure 1) is 15.26 Å, which is slightly bigger than the dithiolene-based 2D sheet (14.62 Å).[30] This is also reflected in the increased pore size with respect to the dithiolene-analogous lattice (12.4 vs 11.9 Å). The values of the optimized bond lengths of Ni−Se, Se−C, and C−C are 2.256, 1.855, and 1.437 (1.412) Å, respectively.

Ethylene is considered to act as a nucleophile in the reactions with dithiolene-like complexes, and it donates π-electrons to the lowest unoccupied molecular orbitals (LUMOs) of the complexes. It was shown that smaller energy differences between the LUMOs of the complexes and the highest occupied molecular orbital (HOMO) of ethylene lead to the increased binding abilities of the complexes.[16] Thus, we analyze and compare the crystal orbitals of 2D $Ni(SeC)_4$ and $Ni(SC)_4$ sheets (Figure S1) obtained with periodic calculations. It turns out that for these two related materials, the crystal orbitals appear to be similar in energies and in spatial distributions. The energy differences between the lowest unoccupied crystal orbital, for sulfur and selenium-based nanosheets, and the HOMO of ethylene are 3.70 and 3.84 eV, respectively. Thus, one could expect a similar reactivity and binding ability of these two 2D materials toward the olefins, based only on the frontier molecular orbitals analysis.

Here, we examine the same binding pattern of ethylene on the 2D $Ni(SeC)_4$ sheet (Figure 2). According to the calculated thermodynamics, the ethylene binding species are labeled as stable adducts (which can be the final products) or intermediates (which are less stable structures, proposed as intermediates but not stable enough to constitute the final products). All the stable adducts refer to the addition of ethylene onto two selenium atoms (a) of adjacent chelate rings of the same Ni center (interligand addition, **2**); (b) of adjacent chelate rings of the same C_6 unit (intraligand addition, **3d**); and (c) within the same chelate ring (intraligand addition, **3s**). For the adducts **2** and **3d**, two related isomers are possible because of the relative orientation of the C−C bond of ethylene with respect to the molecular plane [parallel (**2**, **3d**) vs twisted (**2y**, **3dy**)]. The two intermediates appear as a result of ethylene coordination to the nickel atoms (**4**), or binding across the nickel−selenium bond (**5**). The calculated thermodynamic data of various ethylene-bound species for the $[Ni(SeC)_4]_n$ nanosheet, as well as for the original sulfur-based 2D structure, are compiled in Table 1.

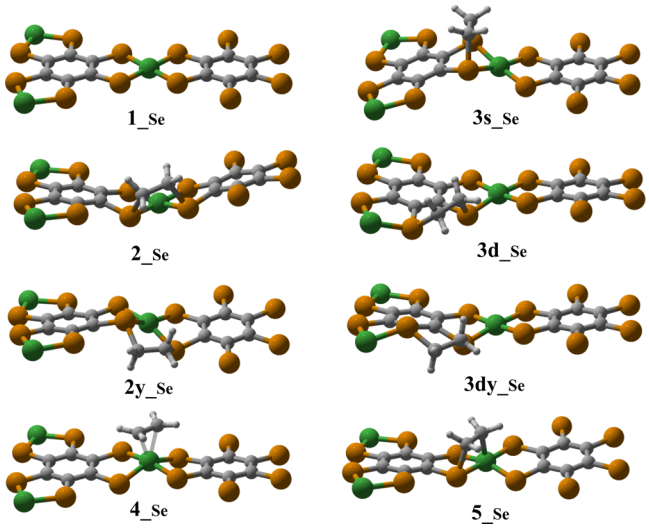

Figure 2. Optimized structures of the relevant species calculated at the HSE06/DZ level. Ni, Se, and C atoms are presented as green, orange-brown, and gray spheres, respectively.

Table 1. Calculated Thermodynamics (kcal/mol) at the HSE06/DZ Level for the $Ni(SC)_4$ and $Ni(SeC)_4$ 2D Sheets[a,b]

structure	2	2y	3s	3d	3dy	4	5
$[Ni(SC)_4]_n$[31]	−21.4	−17.9	−18.2	−18.1	−15.2	3.2	−5.0
$[Ni(SeC)_4]_n$	−17.7	−13.7	−18.0	−16.3	−11.3	0.7	−6.7

[a]All energies are relative to the separated reactants, 1 and ethylene. [b]Negative sign denoted that a product is more stable than the reactants.

For the $Ni(SeC)_4$ sheet system, the thermodynamically most stable species is the intraligand adduct $\mathbf{3s}_{Se}$, which is almost isoenergetic to the interligand adduct $\mathbf{2}_{Se}$ (−18.0 vs −17.7 kcal/mol). The adduct $\mathbf{3d}_{Se}$ is slightly less stable (−16.3 kcal/mol with respect to the separated reactants, $\mathbf{1}_{Se}$ and ethylene). As these three adducts possess very similar stabilities, all can be considered as the potential thermodynamic products of the reaction between $\mathbf{1}_{Se}$ and ethylene. Compared to the planar products, the formation of twisted isomers $\mathbf{2y}_{Se}$ and $\mathbf{3dy}_{Se}$ would be less exothermic (Table 1). On the other hand, the $\mathbf{4}_{Se}$ and $\mathbf{5}_{Se}$ intermediates are considerably less stable, with the former being slightly endothermic (by 0.7 kcal/mol). By comparing the relative stabilities of the two thermodynamic products associated with $Ni(SC)_4$ and $Ni(SeC)_4$ lattices (hereafter denoted as $\mathbf{1}_S$ and $\mathbf{1}_{Se}$), it can be noticed that the first one is 3.4 kcal/mol more stable than the second one ($\mathbf{2}_S$ vs $\mathbf{3s}_{Se}$). Furthermore, all $\mathbf{1}_S$/ethylene adducts are slightly more stable than the $\mathbf{1}_{Se}$/ethylene adducts (Table 1). In contrast, the intermediates **4** and **5** are slightly more stable with $\mathbf{1}_{Se}$.

Regarding the kinetics of the process, different pathways were considered, as depicted in Figure 3. The mechanisms are labeled mainly as "direct" (when the Se atoms directly bind the target carbon atoms) and "indirect" (when an intermediate is formed by ethylene coordination to a Ni atom). As previously found in the sulfur-bearing ($\mathbf{1}_S$) periodic system, the direct formation of **2** with a single transition state is possible through an appropriate transition state $\mathbf{TS}_2$. This contrasts with the molecular system, where the Fan−Hall mechanism through **2y** was proposed, because of the inadequate orbital symmetries.[11] Both mechanisms are studied here and appear to be competitive, with the rate-determining steps of 18.6 ($\mathbf{TS}_{2\_Se}$) and 18.2 kcal/mol ($\mathbf{TS}_{2y}$ from $\mathbf{2y}_{Se}$). The direct formation of the intraligand adducts $\mathbf{3s}_{Se}$ and $\mathbf{3d}_{Se}$ have significantly lower barriers, with the activation energies of 6.3 and 5.6 kcal/mol, respectively.

On the other hand, the indirect mechanism begins with the coordination of ethylene to a nickel center, to form $\mathbf{4}_{Se}$, with an activation barrier of only 6.0 kcal/mol (Figure 3). A subsequent rearrangement into the intermediate $\mathbf{5}_{Se}$ (with a Ni−Se coordination) is an exothermic (−6.0 kcal/mol) and

DOI: 10.1021/acs.jpcc.8b05707
J. Phys. Chem. C 2018, 122, 22424−22434

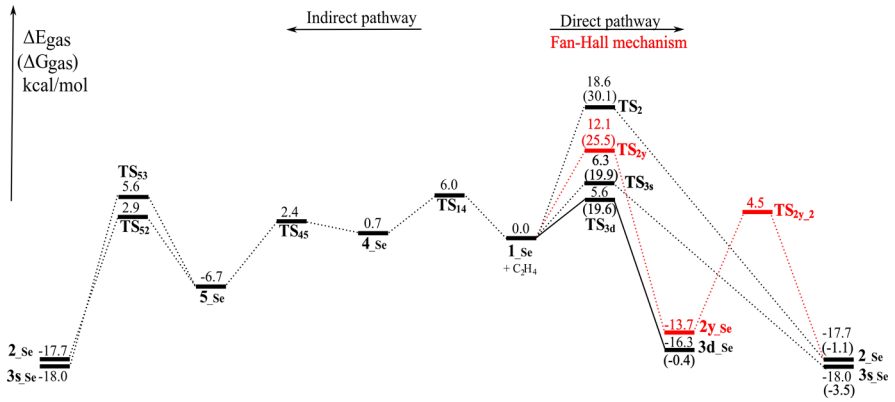

Figure 3. Energy profiles for the reaction of $\mathbf{1}_{Se}$ with ethylene via direct and indirect pathways (black plateaus), as well as for the Fan−Hall mechanism (red plateaus), calculated at the HSE06/DZ level.

very fast process (with a barrier of 1.7 kcal/mol). This intermediate can isomerize into both $\mathbf{2}_{Se}$ and $\mathbf{3s}_{Se}$ adducts, by overcoming the barriers of 9.6 kcal/mol ($\mathbf{TS}_{52}$) and 12.3 kcal/mol ($\mathbf{TS}_{53}$), respectively (Figure 3). In this step, there is a low kinetic selectivity toward the formation of the interligand adduct $\mathbf{2}_{Se}$, with a difference of 2.7 kcal/mol in the barriers.

In summary, the preferred/low energy route is the direct pathway to the formation of $\mathbf{3d}_{Se}$ with an overall barrier of 5.6 kcal/mol. In other words, $\mathbf{3d}_{Se}$ is the kinetic product of the reaction. However, the direct route to $\mathbf{3s}_{Se}$ imposes only 0.7 kcal/mol higher barrier (5.6 vs 6.3 kcal/mol), so these processes are expected to be highly competitive, and a kinetic selection would be difficult. On the other hand, $\mathbf{3s}_{Se}$ is the preferred thermodynamic product of the reaction. The formation of $\mathbf{2}_{Se}$ can be considered as noncompetitive, owing to the much higher rate-determining step barriers of the three pathways: Fan−Hall (18.2 kcal/mol), direct (18.6 kcal/mol), and indirect (9.6 kcal/mol). However, because of the low-barrier formation of the stable intermediate $\mathbf{5}_{Se}$ and its moderate selectivity toward $\mathbf{3s}_{Se}$, the formation of some $\mathbf{2}_{Se}$ cannot be ruled out. Therefore, all adducts are accessible, which would make the product of reaction between $\mathbf{1}_{Se}$ and ethylene mixture.

By comparing the reaction profile of $\mathbf{1}_{Se}$ with the previously published profile for $\mathbf{1}_{S}$, it can be deduced that the two materials display similar patterns for the reaction with ethylene.[31] This can be viewed through the similar barrier heights for the formation of respective adducts, as well as through their similar thermodynamic stabilities. From this perspective, both 2D materials might be considered as potential heterogeneous catalysts for olefin purification, without giving precedence to any. This is the reason why we keep investigating both materials in the following sections, presenting the results for $\mathbf{1}_{Se}$ and $\mathbf{1}_{S}$ in the main text and in the Supporting Information, respectively.

In order to estimate the influence of entropy on the ethylene binding to $\mathbf{1}_{Se}$, we employed cluster models and calculated gas-phase free energies for the most species that constitute the direct pathway at 298.15 K, within the harmonic potential approximation at stationary points, keeping the same level of theory used in PBC calculations (Figure S2a). The estimated Gibbs free energy changes were then calculated by adding the corrections (Δ^{corr}) to the enthalpies obtained from the periodic calculations

$$\Delta^{corr} = (G_{gas} - E_{gas})^{cluster}$$

It can be seen from the diagram that after the inclusion of these corrections to account the entropy contributions of ethylene bindings (∼15 kcal/mol), all adducts are still stabilized. The kinetic product $\mathbf{3d}_{Se}$ has almost zero free-energy change (−0.4 kcal/mol) though, as a consequence of the compensation between the binding enthalpy and the entropy loss, whereas the thermodynamic product $\mathbf{3s}_{Se}$ is 3.5 kcal/mol more stable than the separated reactants. On the other side, the effect of entropy on the kinetics is slightly less pronounced (∼13 kcal/mol), but it still considerably destabilizes the transition states. Nevertheless, the activation energies are lower than 20 kcal/mol ($\mathbf{TS}_{3d}$ and $\mathbf{TS}_{3s}$) and may be considered as moderated and surmountable even at the room temperature. Thus, it can be concluded that this material would display effective olefin binding despite the substantial entropy loss.

Beside their abilities to bind olefins, these catalysts should also be capable to release them upon reduction, which is one of the main requirements for the olefin separation process. It has been shown that for the analogous molecular systems (dithiolene-like complexes), the reduction to the anionic complexes drives the ethylene detachment, which makes the whole process electrochemically controllable.[6] As the inclusion of charges in PBC is quite a challenging task, we investigated the reduction of $\mathbf{1}_{Se}/(C_2H_4)$ adducts using the cluster models. Our previous results, considering $\mathbf{1}_{S}$, have shown that the multiple electron addition is needed to make the mono-ethylene adducts unstable and thereby make the reaction of ethylene release exothermic.[31] Here, we employed similar clusters as used for the prediction of the entropy effect of ethylene adsorption, in order to examine the ethylene release process of $\mathbf{1}_{Se}$ in detail (Figure S2b). We started with the saturated cluster up to coverage 1 (5 C_2H_4 coordinated in 2y fashion per 5 Ni atoms), gradually removed the ethylene molecules one by one, and calculated the thermochemistry of the successive steps. It turns out that the single-electron reduction is sufficient to make the reaction of the first ethylene detachment exothermic (eq 1). However, the release of the second molecule of ethylene would require an injection of two additional electrons (eq 2). Upon the release of the second ethylene molecule, successive dissociations of other ethylene molecules would be performed by spontaneous processes, eqs 3−5 (see also eqs 6−13; Supporting Information). According to the fact that these clusters contain five nickel centers, and only three electrons are needed for all ethylene molecules to be detached, it can be concluded that this catalytic step would be

DOI: 10.1021/acs.jpcc.8b05707
J. Phys. Chem. C 2018, 122, 22424−22434

more cost-effective compared to the molecular systems (1 e^- per 1 Ni). However, it should be noted that these results were obtained using the small cluster systems, and more accurate predictions may be achieved by employing the bigger clusters.

$$[2y_{SC}(C_2H_4)_5]^- \rightarrow [2y_{SC}(C_2H_4)_4]^- + C_2H_4 \quad \Delta H = -2.4 \text{ kcal/mol} \quad (1)$$

$$[2y_{SC}(C_2H_4)_4]^{3-} \rightarrow [2y_{SC}(C_2H_4)_3]^{3-} + C_2H_4 \quad \Delta H = -10.7 \text{ kcal/mol} \quad (2)$$

$$[2y_{SC}(C_2H_4)_3]^{3-} \rightarrow [2y_{SC}(C_2H_4)_2]^{3-} + C_2H_4 \quad \Delta H = -12.5 \text{ kcal/mol} \quad (3)$$

$$[2y_{SC}(C_2H_4)_2]^{3-} \rightarrow [2y_{SC}(C_2H_4)]^{3-} + C_2H_4 \quad \Delta H = -4.1 \text{ kcal/mol} \quad (4)$$

$$[2y_{SC}(C_2H_4)]^{3-} \rightarrow [2y_{SC}]^{3-} + C_2H_4 \quad \Delta H = -1.2 \text{ kcal/mol} \quad (5)$$

We also theoretically predicted the standard redox potentials needed to reduce the $[2y_{SC}(C_2H_4)_5]$ adduct and compared it with the experimentally measured reduction potentials of some related dithiolene complexes. The calculations were carried out in solution, using a solvation model based on density, on the basis of Born−Haber cycle[42] to approximate the experimental conditions reported for the corresponding nickel bis(dithiolene)/olefin systems.[43] The calculated E^0 for the half reaction $[2y_{SC}(C_2H_4)_5] + e^- \rightarrow [2y_{SC}(C_2H_4)_5]^-$ is −1.48 V with respect to Fc/Fc^+, which is very close to the experimentally determined value for the $[Ni(S_2C_2(CF_3)_2)_2]$ (norbornene)/(norbornadiene) systems (−1.32 V).[43] The E^0 values for the half reactions that refer to the addition of second and third electrons are −1.68 and −2.49 V, respectively. These results show that the electrochemical steps of reduction cost a similar amount of energy as those for dithiolene complexes, although this should be taken with caution, considering the fact that the 2D material was approximated with a cluster model.

As it was already mentioned in the Introduction section, one of the practical limitations for the usage of certain catalysts for olefin purification is their poisoning by common impurities (H_2O, H_2S, CO, and C_2H_2). One would expect that the molecules which possess an electron-rich center, such as CO and C_2H_2, should also exhibit strong binding activities to these surfaces. To this end, we studied the tendencies of these two molecules to interact with **1**$_{Se}$. It turns out that carbon monoxide is not able to form any adducts with this surface because every attempt to optimize any CO-bounded species led to the complete detachment of the CO molecule. In contrast, our results have indicated that acetylene would interact strongly with **1**$_{Se}$, by forming adducts that are even more stabilized as compared to the analogous **3d**$_{Se}$ and **3s**$_{Se}$ species (Figure S3). However, we have also found that the activation barriers for acetylene adsorption appear to be about 4 kcal/mol higher in energy than the analogous barriers for the ethylene approach (Figure S3). Therefore, a selective olefin binding to these catalysts might be achieved under well-controlled reaction conditions.

Decomposition Model. In molecular systems, the result of intraligand addition of an olefin onto the nickel bis(dithiolene) complexes (adduct **3**) undergoes a decomposition into a heterocyclic ethylene-dithiolene adduct (**DHD**, i.e. dihydro-1,4-dithiine), and a series of metal-containing species (**MD**).[10] As the main products of the reaction between **1**$_{Se}$ and ethylene are intraligand adducts **3s**$_{Se}$ and **3d**$_{Se}$, it is of great importance to examine the probability of **DHD**-related fragments to detach from the lattice, which would lead to the damage to the material. The same potential risk exists in the **1**$_S$ nanosheet, considering that the related adducts (**3s**$_S$ and **3d**$_S$) would also be formed in the reaction with ethylene (Table 1).[31] In molecular systems, the selenium-containing intermediates have shown a higher stability toward decomposition.[18]

In the extended lattices, the coordination of one ethylene is expected not to lead to the detachment of certain segments from the lattice, which is strengthened by the morphology of the system. This is also true for the low-coverage approach studied until now, with one olefin for the three-nickel unit cell (coverage 1/3). However, when an increased coverage of the surface is considered, such as triple coordination of ethylene in the unit cell (coverage 1), it might lead to the decomposition of the material (Figure 4).

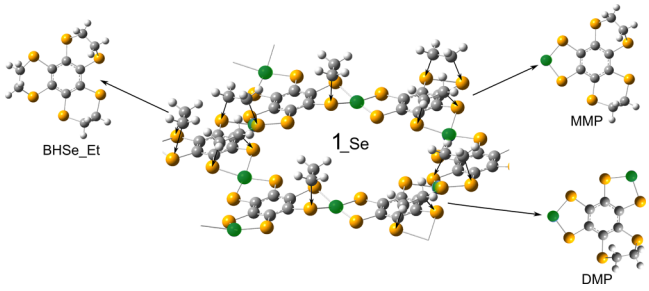

Figure 4. Decomposition scheme of the triple ethylene coordinated **1**$_{Se}$. Ni, Se, and C atoms are presented as green, orange-brown, and gray spheres, respectively.

Hence, we first optimized the structure of intraligand adducts **3s** and **3d** for both materials, by saturating it with three ethylene molecules per three-nickel unit cell, to achieve the coverage of 1 (Figure 5a). Optimized geometries for the analogous dithiolene species are presented in the Supporting Information. For **3s** coordination, there are two ways of binding three ethylene molecules to the repeat unit cell, given the restrictions of having only one ethylene molecule per $NiSe_4$ fragment, and of maintaining the translation symmetry with the three-ethylene unit cell. In the first case, two ethylene molecules are attached to the same benzenehexa-selenol(thiol) unit (BHS), whereas the third ethylene is coordinated to the adjacent BHS unit (**3s**_Se_A″, **3s**″$_{S\_A}$). In the second case, all the three ethylene molecules are coordinated to the same BHS unit (**3s**″$_{Se\_B}$, **3s**″$_{S\_B}$), and the adjacent units have none. On the other side, only one way of triple ethylene binding in a **3d** fashion is considered, which would potentially result in the decomposition, because the three ethylene molecules surround one C_6 unit (**3d**″$_{Se}$, **3d**″$_S$). The relative stability of **3s**″$_{Se\_A}$, with respect to the separated reactants (**1**$_{Se}$ and ethylene), is much higher than the **3s**″$_{Se\_B}$ (−47.0 vs −13.9 kcal/mol), as a consequence of the higher distortion energy introduced in the lattice by the third ethylene coordination to the same BHS unit of latter structure. The same trend was observed for **1**$_S$ nanosheet (Figure S4).

DOI: 10.1021/acs.jpcc.8b05707
J. Phys. Chem. C 2018, 122, 22424−22434

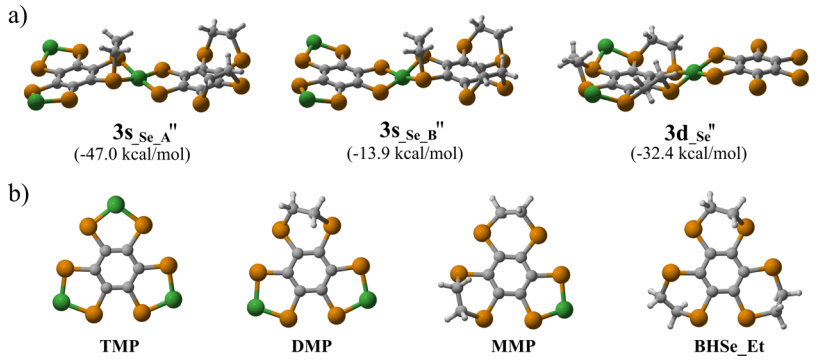

Figure 5. (a) Optimized geometries of triple-coordination intraligand products, calculated at the HSE06/DZ level. Relative stabilities with respect to the separated reactants (**1**$_{Se}$ + 3 molecules of ethylene) are given in brackets. (b) Plausible decomposition species. Ni, Se, and C atoms are presented as green, orange-brown, and gray spheres, respectively.

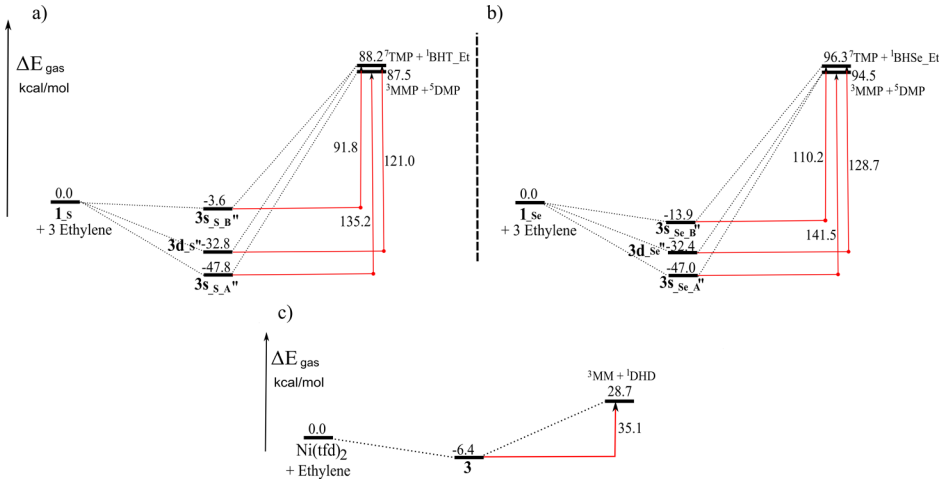

Figure 6. Energy surfaces for the model decomposition process of intraligand adducts for **1**$_S$ (a) and **1**$_{Se}$ (b) 2D sheets, as well as for the original nickel bis(dithiolene) complex ($Ni(tfd)_2$) (c), computed at the HSE06/DZ level of theory. All reported species are in their most stable form.

For the metal bis(dithiolene)-like complexes, it is believed that the first step of the decomposition process is the de-coordination of one of the dithiolene ligand with attached olefin from the metal center, which results in an unsaturated metal monomer (**MM**) and the cyclic product (**DHD**). The relative stability of this species can be used to estimate the feasibility of the decomposition process. However, the use of an unsaturated **MM** is not a good approximation of the overall thermochemistry of the process, which is driven by the formation of metal aggregates. The energy of the initial step (to form the monomer) is thus used as an estimate of the kinetics of the mechanism, as it describes the energy of an unstable intermediate step. In a similar way, the initial products can be described for the 2D extended materials. The **3s″**$_{Se(S)\_A}$ might decompose forming both dimetallic (**DMP**) and monometallic (**MMP**) species, whereas **3s″**$_{Se(S)\_B}$ and **3d″**$_{Se(S)}$ might both decompose through the three-metallic species (**TMP**), and benzenehexa-selenol(thiol) capped with three ethylene molecules (**BHS_Et**) (Figure 5b). Considering the stabilities of these intermediate products, which govern the thermodynamic "barriers" for decomposition, it was shown that for each of them, the most stable form is the one with high multiplicity, describing two unpaired electrons for each unsaturated metal. This indicates that the **MMP**, **DMP**, and **TMP** species are most stable in their triplet, quintet, and septet states, respectively (Table S1).

The calculated energy profiles for the model decomposition process of **3s″** and **3d″** for both (**1**$_{Se}$ and **1**$_S$) nanosheets are compared with the related decomposition profiles for intraligand adduct **3** of the original nickel bis(dithiolene) complex (Figure 6). The adducts are much more stable as compared to the decomposition products in all the three 2D sheets, which make the relative barriers for the decomposition significantly higher with respect to the original complex ($Ni(tfd)_2$). According to this simplified decomposition model, the predicted thermodynamic costs are in the range from 91.8 to 135.2 kcal/mol and from 110.2 to 141.5 kcal/mol for **1**$_S$ and **1**$_{Se}$, respectively. On the other hand, the same simplified model appears to be much more favorable (35.1 kcal/mol) as calculated at the same level of theory in a Ni complex that is experimentally known to decompose (Figure 6c).[10] Thus, it can be concluded that both nanosheet materials would not decompose in reaction with olefins, avoiding a central problem with the original nickel-based complex.

Bilayer Structures. According to a previous DFT study, the Ni bis(dithiolene)-based 2D sheet (**1**$_S$) exists as a bilayer structure rather than in the single-layer form.[32] Furthermore, the same reference also indicated that the most stable configuration is the eclipsed one, owing to the strongest van der Waals attraction, as a result of the maximal overlapping of the two molecular slabs. Such a structure has the biggest possible pores, defined by the molecular architecture of the

DOI: 10.1021/acs.jpcc.8b05707
J. Phys. Chem. C 2018, 122, 22424−22434

individual nanosheet, which would be advantageous for utilizing this material. Hence, we optimized the bilayer structures for both lattices ($\mathbf{1}_{Se}$ and $\mathbf{1}_{S}$) in their eclipse conformations and examined their abilities for the ethylene binding (Figures 7 and S5). However, unlike the $\mathbf{1}_{S}$ bilayer

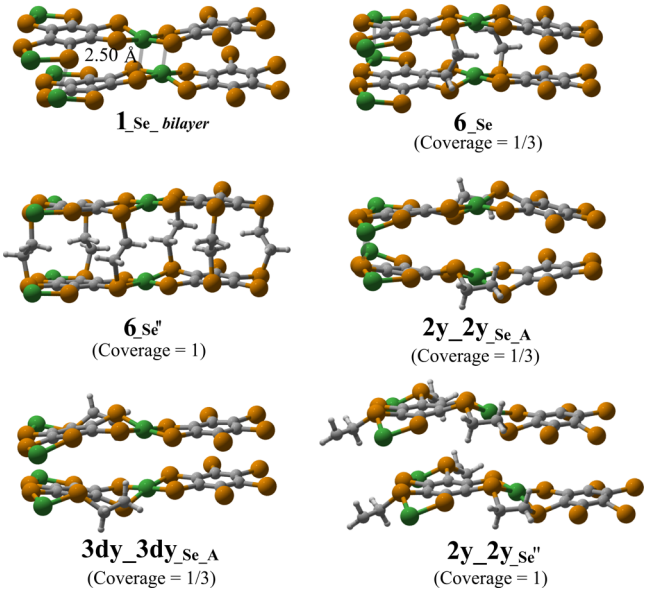

Figure 7. Structure of the bilayer nanosheet ($\mathbf{1}_{Se\_bilayer}$) as well as the selected ethylene adducts, all optimized at the HSE06/DZ level.

structure, the two $\mathbf{1}_{Se}$ nanosheets are not arranged in a perfectly eclipsed conformation, but in a slightly displaced one, with close nickel−selenium contacts settled at a distance of 2.50 Å (Figure 7).

As the double-layer PBC unit cell consists of six nickel atoms, six ethylene molecules were included to achieve the maximum coverage of molecular and monolayer systems (1 Et/1 Ni). First, we examine the new ethylene binding modes that are enabled by the arrangement of bilayer structures, precisely those in which the ethylene molecules connect two stacked molecular sheets (**6**) (Figures 7 and S5).

There is a considerable rise in the stability of such structures by the increase of saturation with ethylene molecules per unit cell (Table 2). The attachment of two ethylene molecules to a double-layered unit cell, which corresponds to the coverage of 1/3, would yield to adduct $\mathbf{6}_{Se}$ that is 25.3 kcal/mol more stable as compared to the separated reactants. Further saturation with ethylene molecules, up to coverage 1, would enormously increase the stabilization of adduct $\mathbf{6}''_{Se}$ (−121.1 kcal/mol). In this structure, there are six ethylene molecules coordinated per unit cell that adjust the distance between the two molecular slabs, which are no longer in close contact (the average distance is about 5 Å). Hence, the energy contribution from the ethylene binding wins over the stabilization by stacking of the $\mathbf{1}_{Se\_bilayer}$ structure. As is usual, we failed to optimize any structure which exceeds coverage 1 (with more ethylene molecules than nickel atoms) for the $\mathbf{1}_{Se\_bilayer}$. On the other hand, we succeeded in optimizing one structure that exceeds coverage 1 for the $\mathbf{1}_{S\_bilayer}$, with eight ethylene molecules coordinated per unit cell (Figure S5; $\mathbf{6}'''_{S}$), but it is unstable when compared to the adduct $\mathbf{6}''_{S}$ with coverage 1 (Table 2). The two additional ethylene molecules were added along the nickel−sulfur bonds on different sides of the two sheet planes, with a very distorted geometry around the Ni coordination center of one sheet (breaking the Ni−S bond).

Table 2. Calculated Thermodynamics (kcal/mol) at the HSE06/DZ Level for the $\mathbf{1}_{Se\_bilayer}$ and $\mathbf{1}_{S\_bilayer}$ Ethylene Adducts with Different Coverage

	coverage	$\mathbf{1}_{Se\_bilayer}$	$\mathbf{1}_{S\_bilayer}$
6	1/3	−25.3	−49.6
6′	2/3	−50.6	−76.9
6″	1	−121.1	−103.1
6‴	4/3	[a]	−74.8
2y_2y_A	1/3	−31.4	−38.6
2y_2y_B	1/3	−25.2	−39.6
2y_2y″	1	−59.3	−87.0
2y_3dy	1/3	−21.4	−40.1
3dy_3dy_A	1/3	−32.9	−38.3
3dy_3dy_B	1/3	−20.0	−47.5

[a]We failed to optimize the adduct **6_Se‴**.

Because of the variety of binding modes possible in a bilayer structure, we did not examine all of them in detail. We discuss here only the twisted adducts (**2y**, **3dy**) because it turns out that the parallel adducts **2** and **3d** are less thermodynamically stable in the multilayer structure because of the steric clashing of coordinated ethylene molecules of the lower layer with the molecular plane of the upper layer. For the same reason, the binding motif **3s** is not considered for the multilayer calculations. The structures with two coordinated ethylene molecules, that is, one per each sheet (coverage = 1/3), are all stable, with the binding energies ranging from 20 to 33 kcal/mol for $\mathbf{1}_{Se\_bilayer}$ and from 38.3 to 47.5 kcal/mol for $\mathbf{1}_{S\_bilayer}$ (Table 2). These products display different stabilities, depending on the position of the ethylene binding. In order to describe different products in a systematic way, we used a specific name convention. Thus, here **2y_2y_A** refers to the structure in which there is one ethylene molecule bound to each molecular sheet, both in the twisted arrangement **2y**, and coordinated on the opposite sides of the two stacked chelates. In contrast, the subscript "_B" denotes that the coordination is on the same side of the stacked chelates (e.g., **2y_2y_B** as shown in Figure S5). The notation **2y_2y″** denotes the structures with the coverage equivalent to the molecular system (1 Et/1 Ni) with energies of −59.3 and −87.0 kcal/mol for the selenium and sulfur bilayer structures, respectively. Unlike $\mathbf{1}_{S\_bilayer}$ adducts, which all have eclipse structure, some of the $\mathbf{1}_{Se\_bilayer}$ adducts (**2y_2y_B**, **3dy_3dy_B**) have *offset* slipped-parallel arrangement of the molecular slabs, which is reflected in the lower stability, owing to the decreased overlapping of the two sheets, and thereby to reduced van der Waals interactions. Nevertheless, taking everything into account, it can be concluded that both π-conjugated 2D materials ($[Ni(SC)_4]_n$ and $[Ni(SeC)_4]_n$), in their bilayer form, are potential heterogeneous catalysts for olefin separation. The data indicate that the efficiency of these materials for olefin bindings is at least the same as for the molecular complexes.

3D Structures. In the previous sections, we considered the attachment of ethylene molecules to the mono- and bilayer $[Ni(XC)_4]_n$ (X = S, Se) nanosheets. In this section, we consider novel 3D structures of infinitely stacked nickel dithiolene and diselenolene-based nanosheets, as well as their abilities for ethylene binding. Note that these 3D systems have not appeared in previous works. Despite not being experimentally confirmed, the existence of these motifs as

DOI: 10.1021/acs.jpcc.8b05707
J. Phys. Chem. C 2018, 122, 22424−22434

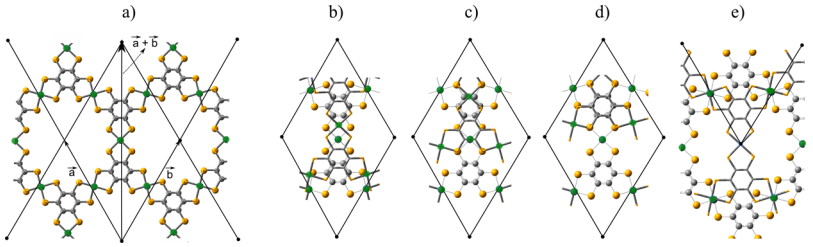

Figure 8. Top view of the different conformations of hypothetical 3D $Ni(SeC)_4$ sheets, which were constructed by gradual sliding along the diagonal direction. (a) Eclipsed, (b–d) intermediate, and (e) maximum displaced structure. Two primitive vectors ($\vec{a}$, $\vec{b}$), the primitive cell defined by these vectors, and the diagonal direction along the ($\overrightarrow{a+b}$) are also presented.

polylayer 3D forms will be relevant in the practical application of these materials, and thus, it is of interest to examine the ability of such 3D structures to bind olefins. First, we tried to predict the most stable configuration of $[Ni(XC)_4]_n$ polylayer materials, in terms of the relative position of stacked slabs. Thus, we investigated the changes of overall energies with respect to the shift between the layers. Namely, series of single point calculations have been performed, based on the conformations that we generated, by a gradual increase of the displacement between the stacked sheets along the diagonal direction ($\overrightarrow{a+b}$), starting from the eclipse conformation (Figure 8a). This direction, defined as the sum of the two translation vectors, ($\overrightarrow{a+b}$), corresponds to the direction connecting the Ni with the center of an adjacent C_6 ring. After the eclipsed conformation, in the second constructed conformation, the sheets were slid by 1.89 Å, and nickel atoms from one layer are positioned above and below the centroid of the respective chelate rings (Figure 8b). Further displacement along the diagonal direction led to the third conformation in which there is the maximal overlapping between the chelate and C_6 rings (Figure 8c). In the fourth conformation, the C_6 rings from the neighboring sheets are in the *face-to-face* conformation (Figure 8d). By increasing the sliding between the sheets, $Ni(SeC)_4$ fragments from one layer gradually cover the large pore of another layer. The last constructed geometry is one with the minimal possible overlay of the atoms from the stacked molecular slabs. In this conformation, $Ni(Se_2C_6)_2$ as well as $Ni(S_2C_6)_2$ fragments from one sheet are almost perfectly positioned above the large pore of adjacent sheets, and such an arrangement of the molecular slabs would yield a structure with the smallest possible apertures (Figure 8e).

Figure 9 shows the relative electronic energies of the examined conformations with respect to the starting geometry (eclipsed), plotted versus the displacement along the $\overrightarrow{a+b}$ vector (Å), for the $[Ni(SC)_4]_n$ and $[Ni(SeC)_4]_n$ 3D structures. Any sliding along the diagonal direction leads to less stable structures, as compared to the eclipsed geometry. The first two conformations are the most unfavorable, with relative energies that are 50.2 and 53.1 kcal/mol higher than the eclipsed conformation for $[Ni(SeC)_4]_n$. A further displacement of the sheets leads to more stable conformations, but significantly destabilized in comparison with the eclipsed geometry (Figure 9). The same trend is observed for $[Ni(SC)_4]_n$ sheets, but the destabilization is smaller. We have also considered the geometries obtained by displacements along the Ni–Se or Ni–S bonds, with close nickel–selenium or nickel–sulfur contacts (Figure S6). Despite being more stable than the

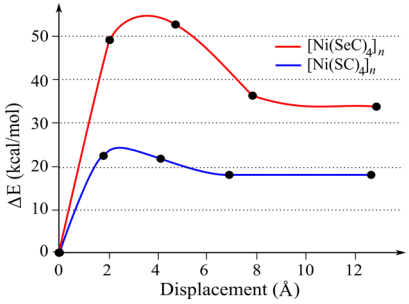

Figure 9. Relative electronic energies with respect to the eclipse geometries, calculated using the HSE06/DZ level of theory, plotted as a function of the diagonal displacement between sheets, for the two hypothetical 3D materials.

($\overrightarrow{a+b}$) slid examples mentioned above, such arrangements of the layers are also less favorable relative to the eclipsed conformation (ΔE = 20.3; 9.9 kcal/mol). In order to confirm that our predictions about the preferred arrangement of the sheets in the hypothetical 3D network are not an artifact of the methodology, we performed additional calculations for the $[Ni(SC)_4]_n$ 3D system with the M06-L functional, which implicitly includes dispersion.[38] There are significant differences in the energy/displacement curves obtained with both functionals, but they are consistent with the fact that the eclipsed conformation is the most stable geometry for the 3D materials (Figure S7). These results can be explained by the maximal possible overlay of the sheets in the eclipsed interaction, which causes the strongest van der Waals and π-stacking interactions.

Because of the computational costs associated with the 3D periodic calculations, only two adducts of diselenolene-based polylayer sheets were optimized, based on our results in bilayer calculations. The results indicate that the ethylene binding, in twisted fashions (**2y** and **3dy**) to the eclipsed $[Ni(SeC)_4]_n$, would yield in unstable adducts, with the relative energies to the separated reactants of 16.3 and 9.3 kcal/mol, respectively (Figure 10). On the other hand, the same adducts of the $[Ni(SC)_4]_n$ 3D structure are more stable (**2y** = 0.3 kcal/mol; **3dy** = −5.9 kcal/mol, Figure S8), probably because of the higher flexibility of the dithiolene-based framework. However, none of these adducts can be considered as stable products, as these are potential energy calculations and the entropy of releasing the olefin will probably beat a stabilization of less than 6 kcal/mol. For $[Ni(SC)_4]_n$, different coordination motifs were explored, looking for a stable product, and two additional adducts were found (**2** and **3d**; Figure S8), with higher thermodynamic stabilities (−12.7 and −6.7 kcal/mol for **2** and **3d**, respectively). Hence, the results using this model suggest

DOI: 10.1021/acs.jpcc.8b05707
J. Phys. Chem. C 2018, 122, 22424–22434

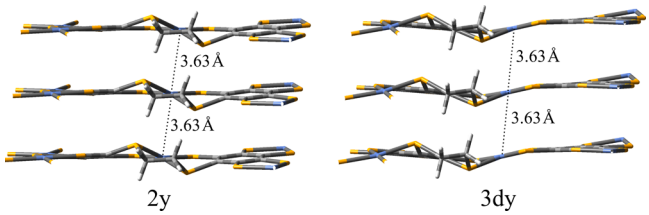

Figure 10. Optimized structures of two ethylene adducts associated with $[Ni(SeC)_4]_n$ 3D sheets calculated at the HSE06/DZ level.

that this 3D material is probably not able to form stable adducts. Overall, it is difficult to judge whether these 3D materials could be used as heterogeneous catalysts for olefin separation. On the other hand, the high porosity of these materials imposed by an eclipsed architecture may indicate effective olefin bindings and ease the practical use of these materials.

CONCLUSIONS

In this study, we investigated the structural and electronic properties and their reactivity toward the ethylene coordination of 2D and 3D $[Ni(XC)_4]_n$ (X = Se and S) sheets, using the first-principles calculations, namely a previously selected screened hybrid density functional. The optimization of nickel bis(diselenolene)-based nanosheets reveals that the structure of porous cross-linked planar $Ni(SeC)_4$ network is similar to the previously determined structure of dithiolene-based nanosheets, with slightly larger pore size.

The comparison of reaction profiles of monolayers of $[Ni(SeC)_4]_n$ with ethylene indicated that they are similar to those calculated for the analogous $[Ni(SC)_4]_n$, as well as for the related molecular complexes. The most favorable pathway is the direct route that leads to the formation of intraligand adduct $\mathbf{3d}_{\mathbf{Se}}$ (a kinetic product), which has a slightly lower activation barrier than the thermodynamic product of the reaction ($\mathbf{3s}_{\mathbf{Se}}$). The comparison with the dithiolene-based 2D sheet shows that they have the same kinetic product, but the reaction barrier is lower for $Ni(SeC)_4$ (5.6 vs 8.1 kcal/mol). In contrast, the thermodynamic products are different ($\mathbf{3s}_{\mathbf{Se}}$ vs $\mathbf{2}_{\mathbf{S}}$), though similar in stability. However, all the species are accessible because of the similar barrier heights and relative stabilities, which indicate that the final product of the reaction would be a lattice with ethylene molecules attached to the various positions. Therefore, $[Ni(SeC)_4]_n$ in the single-layer form might be considered as a potential heterogeneous catalyst for olefin purification, with a similar performance as the previously published $Ni(SC)_4$.

One of the main disadvantages of using the original homogeneous catalyst nickel bis(dithiolene) for olefin purification is its tendency to decompose in the presence of olefins. The decomposition is the result of the intraligand addition of olefins, leading to the formation of unstable intraligand adducts **3** that release a cyclic organic molecule. Considering that for the $[Ni(XC)_4]_n$ sheets the intraligand adduct is one of the main products of the reaction, we explored the feasibility of such fragments to detach from the lattice, which would lead to the damage of materials and limit their practical use. By comparing the differences in relative stabilities between the triple ethylene coordinated model (coverage 1) and the respective dissociating species, with those in the molecular systems, it can be concluded that the thermodynamic barriers for decomposition processes would be extremely high for both lattices (>100 kcal/mol). Thus, it can be concluded that both monolayer materials are resistant to decomposition in reactions with olefins, and all adducts are useful, as well as their various combinations.

Regarding the bilayer structures of these lattices, our calculations suggest that the conformation of Ni bis(dithiolene) sheets is eclipsed, whereas analogous diselenolene sheets rather exist in displaced conformations, which have close nickel−selenium contacts. New ethylene binding modes were proposed for both lattices, in which ethylene molecules act as linkers between the stacked sheets. Considering molecular efficiency of these two materials, the data show that the coordination of ethylene molecules in different positions is favored up to coverage 1 (the same as in molecular systems). However, we succeeded in optimizing one adduct of dithiolene-based bilayer sheets, which surpasses the coverage of molecular complexes, with a greater number of coordinated alkenes than nickel atoms. In addition, the weight efficiency of these materials is higher than the molecular systems, owing to the much smaller size of the ligand.

Our investigation concerning hypothetical 3D arrangements of infinitely stacked sheets of these two materials reveals that the most stable conformation is eclipsed, with a vertical alignment of the layers, because of the strongest van der Waals interactions. Such an arrangement of molecular slabs leads to the highly porous materials, which may contribute to effective olefin bindings. Indeed, our calculations show that some of the optimized adducts are quite stable, which might signify the effectiveness of these polylayer forms as potential heterogeneous catalysts for olefin purification.

ASSOCIATED CONTENT

Supporting Information

The Supporting Information is available free of charge on the ACS Publications website at DOI: 10.1021/acs.jpcc.8b05707.

Molecular Orbital analysis; model systems for predicting the ethylene release ability and entropy effects; the energy profile for the reaction of $\mathbf{1}_{\mathbf{Se}}$ with acetylene; the geometries and energies of various metal-decomposition species; the geometries of various bilayer structures; different 3D structures, and the diagram of the relative electronic energies; the optimized geometries and electronic energies of all Se-based species (PDF)

AUTHOR INFORMATION

Corresponding Authors

*E-mail: dusan.sredojevic@qatar.tamu.edu (D.N.S.).
*E-mail: ed.brothers@qatar.tamu.edu (E.N.B.).

ORCID

Dušan N. Sredojević: 0000-0003-2867-2047
Salvador Moncho: 0000-0003-1631-5587
Rajesh Kumar Raju: 0000-0002-0030-3242

Notes

The authors declare no competing financial interest.

ACKNOWLEDGMENTS

This publication was made possible by the Qatar National Research Fund through the NPRP grants 7-665-1-125 and 5-318-1-063. The calculations were performed at the RAAD2 supercomputer at the Texas A&M University at Qatar.

DOI: 10.1021/acs.jpcc.8b05707
J. Phys. Chem. C 2018, 122, 22424−22434

REFERENCES

(1) National Research Council. *Separation and Purification: Critical Needs and Opportunities*; National Academy Press: Washington, DC, 1987.

(2) Sundaram, K. M.; Sreehan, M. M.; Olszewski, E. F. *Kirk-Othmer Encyclopedia of Chemical Technology*, 4th ed.; Wiley: New York, 1995.

(3) Eldridge, R. B. Olefin/paraffin separation technology: a review. *Ind. Eng. Chem. Res.* **1993**, *32*, 2208−2212.

(4) Suzuki, T.; Noble, R. D.; Koval, C. A. Electrochemistry, stability, and alkene complexation chemistry of copper(I) triflate in aqueous solution. Potential for use in electrochemically modulated complexation-based separation processes. *Inorg. Chem.* **1997**, *36*, 136−140.

(5) Kim, H. S.; Kim, H.; Ahn, B. S.; Ryu, J. H.; Kang, Y. S. Reversible olefin complexation by silver ions in dry poly(vinyl methyl ketone) membrane and its application to olefin/paraffin separations. *Chem. Commun.* **2000**, *14*, 1261−1262.

(6) Wang, K.; Stiefel, E. I. Toward separation and purification of olefins using dithiolene complexes: an electrochemical approach. *Science* **2001**, *291*, 106−109.

(7) Wing, R. M.; Tustin, G. C.; Okamura, W. H. Oxidative cycloaddition of metal dithiolenes to olefins. Synthesis and characterization of norbornadiene-bis-cis-(1,2-perfluoromethylethene-1,2-dithiolato)nickel. *J. Am. Chem. Soc.* **1970**, *92*, 1935−1939.

(8) Baker, J. R.; Hermann, A.; Wing, R. M. Mechanism of oxidative cycloaddition of olefins to metal dithiolenes. *J. Am. Chem. Soc.* **1971**, *93*, 6486−6489.

(9) Herman, A.; Wing, R. M. The structure of the nickel bis(1,2-ethenedithiolate)/2,3-dimethylbutadiene cycloaddition reaction product. *J. Organomet. Chem.* **1973**, *63*, 441−450.

(10) Harrison, D. J.; Nguyen, N.; Lough, A. J.; Fekl, U. New Insight into Reactions of Ni(S2C2(CF3)2)2with Simple Alkenes: Alkene Adduct versus Dihydrodithiin Product Selectivity Is Controlled by [Ni(S2C2(CF3)2)2]-Anion. *J. Am. Chem. Soc.* **2006**, *128*, 11026−11027.

(11) Fan, Y.; Hall, M. B. How Electron Flow Controls the Thermochemistry of the Addition of Olefins to Nickel Dithiolenes: Predictions by Density Functional Theory. *J. Am. Chem. Soc.* **2002**, *124*, 12076−12077.

(12) Dang, L.; Yang, X.; Zhou, J.; Brothers, E. N.; Hall, M. B. Computational studies on ethylene addition to nickel bis(dithiolene). *J. Phys. Chem. A* **2012**, *116*, 476−482.

(13) Dang, L.; Shibl, M. F.; Yang, X.; Alak, A.; Harrison, D. J.; Fekl, U.; Brothers, E. N.; Hall, M. B. The mechanism of alkene addition to a nickel bis(dithiolene) complex: the role of the reduced metal complex. *J. Am. Chem. Soc.* **2012**, *134*, 4481−4484.

(14) Dang, L.; Shibl, M. F.; Yang, X.; Harrison, D. J.; Alak, A.; Lough, A. J.; Fekl, U.; Brothers, E. N.; Hall, M. B. Apparent Anti-Woodward-Hoffmann Addition to a Nickel Bis(dithiolene) Complex: The Reaction Mechanism Involves Reduced, Dimetallic Intermediates. *Inorg. Chem.* **2013**, *52*, 3711−3723.

(15) Shibl, M. F.; Dang, L.; Raju, R. K.; Hall, M. B.; Brothers, E. N. A mechanism for the addition of ethylene to nickel bis-dithiolene. *Int. J. Quantum Chem.* **2012**, *113*, 1621−1625.

(16) Li, H.; Brothers, E. N.; Hall, M. B. Computational exploration of alternative catalysts for olefin purification: cobalt and copper analogues inspired by nickel bis(dithiolene) electrocatalysis. *Inorg. Chem.* **2014**, *53*, 9679−9691.

(17) Dang, L.; Ni, S. F.; Hall, M. B.; Brothers, E. N. Uptake of one and two molecules of 1,3-butadiene by platinum bis(dithiolene): a theoretical study. *Inorg. Chem.* **2014**, *53*, 9692−9702.

(18) Raju, R. K.; Sredojevic, D. N.; Moncho, S.; Brothers, E. N. Nickel Bis(diselenolene) as a Catalyst for Olefin Purification. *Inorg. Chem.* **2016**, *55*, 10182−10191.

(19) Sredojevic, D. N.; Raju, R. K.; Moncho, S.; Brothers, E. N. Mechanism of Ethylene Addition to Nickel Bis(oxothiolene) and Nickel Bis(dioxolene) Complexes. *J. Phys. Chem. A* **2016**, *120*, 7561−7568.

(20) *Catalyst Separation, Recovery and Recycling: Chemistry and Process Design*; Cole-Hamilton, D. J., Tooze, R. P., Eds.; Catalysis ByMetal Complexes; Springer: Dordrecht, 2006.

(21) Kambe, T.; Sakamoto, R.; Hoshiko, K.; Takada, K.; Miyachi, M.; Ryu, J.-H.; Sasaki, S.; Kim, J.; Nakazato, K.; Takata, M.; Nishihara, H. π-Conjugated Nickel Bis(dithiolene) Complex Nanosheet. *J. Am. Chem. Soc.* **2013**, *135*, 2462−2465.

(22) Novoselov, K. S.; Geim, A. K.; Morozov, S. V.; Jiang, D.; Zhang, Y.; Dubonos, S. V.; Grigorieva, I. V.; Firsov, A. A. Electric Field Effect in Atomically Thin Carbon Films. *Science* **2004**, *306*, 666−669.

(23) Geim, A. K.; Novoselov, K. S. The Rise of Graphene. *Nat. Mater.* **2007**, *6*, 183−191.

(24) Tang, Q.; Zhou, Z.; Chen, Z. Graphene-related nanomaterials: tuning properties by functionalization. *Nanoscale* **2013**, *5*, 4541−4583.

(25) Watanabe, K.; Taniguchi, T.; Kanda, H. Direct-bandgap properties and evidence for ultraviolet lasing of hexagonal boron nitride single crystal. *Nat. Mater.* **2004**, *3*, 404−409.

(26) Topsakal, M.; Aktürk, E.; Ciraci, S. First-principles study of two- and one-dimensional honeycomb structures of boron nitride. *Phys. Rev. B: Condens. Matter Mater. Phys.* **2009**, *79*, 115442.

(27) Tang, Q.; Zhou, Z.; Chen, Z. Molecular Charge Transfer: A Simple and Effective Route To Engineer the Band Structures of BN Nanosheets and Nanoribbons. *J. Phys. Chem. C* **2011**, *115*, 18531−18537.

(28) Zeng, H.; Zhi, C.; Zhang, Z.; Wei, X.; Wang, X.; Guo, W.; Bando, Y.; Golberg, D. "White Graphenes": Boron Nitride Nanoribbons via Boron Nitride Nanotube Unwrapping. *Nano Lett.* **2010**, *10*, 5049−5055.

(29) Shojaei, F.; Hahn, J. R.; Kang, H. S. Mechanical and Electronic Properties of π-Conjugated Metal Bis(dithiolene) Complex Sheets. *Chem. Mater.* **2014**, *26*, 2967−2974.

(30) Tang, Q.; Zhou, Z. Electronic Properties of π-Conjugated Nickel Bis(dithiolene) Network and Its Addition Reactivity with Ethylene. *J. Phys. Chem. C* **2013**, *117*, 14125−14129.

(31) Moncho, S.; Brothers, E. N.; Hall, M. B. Addition of ethylene to a π-conjugated two-dimensional nickel-based organometallic framework with implications for olefin separation. *J. Mol. Model.* **2015**, *21*, 107.

(32) Shojaei, F.; Kang, H. S. Continuous Tuning of Band Gap for π-Conjugated Ni Bis(dithiolene) Complex Bilayer. *J. Phys. Chem. C* **2014**, *118*, 25626−25632.

(33) Frisch, M. J.; Trucks, G. W.; Schlegel, H. B.; Scuseria, G. E.; Robb, M. A.; Cheeseman, J. R.; Scalmani, G.; Barone, V.; Mennucci, B.; Petersson, G. A.; et al. *Gaussian Development Version*, Revision H.32; Gaussian, Inc.: Wallingford, CT, 2009.

(34) Heyd, J.; Scuseria, G. E.; Ernzerhof, M. Hybrid functionals based on a screened Coulomb potential. *J. Chem. Phys.* **2003**, *118*, 8207−8215; erratum. *J. Chem. Phys.* **2006**, *124*, 219906.

(35) Heyd, J.; Scuseria, G. E. Assessment and validation of a screened Coulomb hybrid density functional. *J. Chem. Phys.* **2004**, *120*, 7274−7280.

(36) Heyd, J.; Scuseria, G. E. Efficient hybrid density functional calculations in solids: Assessment of the Heyd-Scuseria-Ernzerhof screened Coulomb hybrid functional. *J. Chem. Phys.* **2004**, *121*, 1187−1192.

(37) Perdew, J. P.; Burke, K.; Ernzerhof, M. Generalized gradient approximation made simple. *Phys. Rev. Lett.* **1996**, *77*, 3865−3868.

(38) Zhao, Y.; Truhlar, D. G. The M06 suite of density functionals for main group thermochemistry, thermochemical kinetics, noncovalent interactions, excited states, and transition elements: two new functionals and systematic testing of four M06-class functionals and 12 other functionals. *Theor. Chem. Acc.* **2007**, *120*, 215−241.

(39) Weigend, F.; Ahlrichs, R. Balanced basis sets of split valence, triple zeta valence and quadruple zeta valence quality for H to Rn: design and assessment of accuracy. *Phys. Chem. Chem. Phys.* **2005**, *7*, 3297−3305.

DOI: 10.1021/acs.jpcc.8b05707
J. Phys. Chem. C 2018, 122, 22424−22434

(40) Monkhorst, H. J.; Pack, J. D. Special points for Brillouin-zone integrations. *Phys. Rev. B: Solid State* **1976**, *13*, 5188−5192.
(41) Macrae, C. F.; Bruno, I. J.; Chisholm, J. A.; Edgington, P. R.; McCabe, P.; Pidcock, E.; Rodriguez-Monge, L.; Taylor, R.; van de Streek, J.; Wood, P. A. Mercury CSD 2.0- new features for the visualization and investigation of crystal structures. *J. Appl. Crystallogr.* **2008**, *41*, 466−470.
(42) Li, J.; Fisher, C. L.; Chen, J. L.; Bashford, D.; Noodleman, L. Calculation of Redox Potentials and pKa Values of Hydrated Transition Metal Cations by a Combined Density Functional and Continuum Dielectric Theory. *Inorg. Chem.* **1996**, *35*, 4694−4702.
(43) Geiger, W. E. Electrochemistry of Cycloaddition Products of Olefins with Nickel Dithiolenes: A Reinvestigation of the Reduction of the 1:1 Adduct between Ni(S2C2(CF3)2)2and Norbornadiene. *Inorg. Chem.* **2002**, *41*, 136−139.

DOI: 10.1021/acs.jpcc.8b05707
J. Phys. Chem. C 2018, 122, 22424−22434